Synchronized and unsynchronized chaos in a modulated bidirectional ring laser

Fuad Rawwagah,* Baolong Lu,† and Surendra Singh
Physics Department, University of Arkansas, Fayetteville, Arkansas 72701, USA
(Received 18 October 2006; published 16 April 2007)

Regimes of antisynchronized quasiperiodic and synchronized and unsynchronized chaotic oscillations have been observed in a bidirectional solid-state ring laser with modulated pump and are chracterized in terms of the maximum Lyapunov exponent. The results can be understood in terms of the coupled dynamics of two counterpropagating modes of a ring laser coupled to atomic population inversion.

DOI: 10.1103/PhysRevA.75.043811 PACS number(s): 42.65.Sf, 42.60.Mi, 42.55.Ah

Chaotic oscillations are noiselike fluctuations of system variables characterized by a complex power spectrum and extreme sensitivity to initial conditions. Chaotic oscillations are, in fact, a collection of many orderly trajectories, none of which dominates under ordinary circumstances [1]. By perturbing a chaotic system in the right way, we can control chaos [2–4] and force the system to follow one of its regular trajectories [5–7]. Another fascinating aspect of chaotic dynamics is that coupled chaotic systems can synchronize and track each other's chaotic motion [8–10].

Synchronization of periodic oscillations has been known since Huygens' observation of this phenomenon in coupled pendulum clocks [8]. That synchronization can occur also in the regime of chaotic oscillations is a relatively recent realization. Understanding of chaos and mechanisms for its control are of interest not only from the fundamental viewpoint but also for applications of chaotic signals across the spectrum of scientific endeavor ranging from encryption in communication [11] to electronic circuits [12] and control of cardiac function [13].

Using a simple system of two modes of a class-*B* ring laser coupled via the gain medium and backscattering, we predict theoretically and observe experimentally that mode intensities can exhibit periodic and chaotic oscillations. Moreover, in a certain range of parameters, chaotic oscillations of mode intensities synchronize and the laser emits identical copies of the same chaotic signal in two directions. In contrast to most recent studies [11–13], where synchronization arises due to an asymmetric master-slave coupling between two different chaotic systems, in our case, the internal system dynamics self-organizes to produce synchronized chaotic and quasiperiodic oscillations of mode intensities.

The experiments were carried out on a continuous wave neodymium-doped yttrium aluminum garnet (Nd:YAG) solid-state ring laser operating at 1064 nm and pumped by a diode laser operating at 810 nm. An outline of the experimental setup is shown in Fig. 1. The laser cavity consists of two spherical mirrors around a 2-cm-long Nd:YAG gain rod and two flat mirrors arranged to form a folded ring cavity. The end surfaces of the Nd:YAG rod were antireflection coated for the pump and laser wavelengths. A mode-matching lens focused the light from the pump diode laser at the center of the gain rod. A small-amplitude modulation current from a signal generator was added to the diode laser drive current. By varying the amplitude and frequency of modulation current we can modulate the pump intensity and therefore the gain of the ring laser.

The experiments were performed with the ring laser operating in a single longitudinal mode in each direction. The two oppositely directed traveling wave modes are coupled via their competition for gain from the same set of atoms and by the backscattering of radiation from one mode into the direction of the other from various optical elements inside the cavity. The gain medium responds to the total electric field, which is a superposition of the fields of the two modes leading to a spatially varying population density. This system of modes can be described by the following set of equations of motion [14–16]:

$$\dot{f}_1 = (d_0 - 1)f_1 + \left(i\frac{b}{\kappa} + d_+\right)f_2, \tag{1}$$

$$\dot{f}_2 = (d_0 - 1)f_2 + \left(i\frac{b}{\kappa} + d_-\right)f_1, \tag{2}$$

$$\dot{d}_0 = a[r - d_0(1 + |f_1|^2 + |f_2|^2) - d_+ f_1^* f_2 - d_- f_1 f_2^*], \tag{3}$$

$$\dot{d}_+ = a[-d_0 f_1 f_2^* - d_+(1 + |f_1|^2 + |f_2|^2)]. \tag{4}$$

Here f_1 and f_2 are the scaled, dimensionless, slowly varying field amplitudes for the two modes, d_0 is the average population density, and d_+ $(=d_-^*)$ is the complex Fourier amplitude

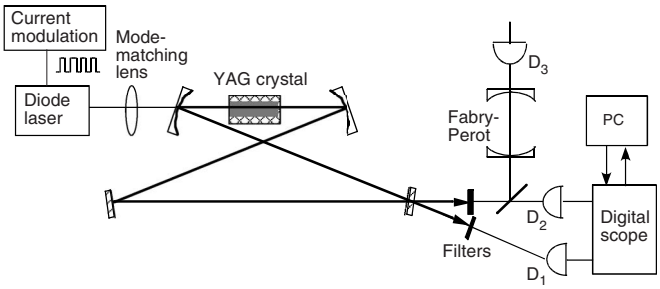

FIG. 1. An outline of the experimental setup.

*Present address: Physics Department, Yarmouk University, Irbid 211-63, Jordan.

†Present address: Center for Cold Atom Physics, Wuhan Institute of Physics and Mathematics, Chinese Academy of Sciences, Wuhan 430071, China.

of the leading spatial harmonic of population density. Both d_0 adn d_+ have been expressed in terms of the average threshold population density. b (rad/s) is the backscattering coefficient, κ (s^{-1}) is the cavity field decay rate, $a=\gamma_\parallel/\kappa$, where $\gamma_\parallel$ is the population decay rate, and time has been scaled in units of κ^{-1}. The pump ratio r is the pump laser power relative to the threshold pump power. For the ring laser operation below threshold $r<1$, and for operation above threshold $r>1$. The pump ratio r was modulated by a square wave signal of amplitude h_m,

$$r = r_0 + h_m \,\mathrm{sgn}[\cos(2\pi\nu_m \tau/\kappa)] \tag{5}$$

where r_0 is the average value of the pump ratio and the function $\mathrm{sgn}(x)$ is +1 if its argument x is positive and −1 if it is negative.

The advantage of scaled dynamical equations is that only two (lumped) parameters b and κ are needed to simulate the behavior of a particular system. We shall see that b and κ can be determined experimentally and, once κ is known, the third parameter $a=\gamma_\parallel/\kappa$ is determined from the knowledge of the population decay rate $\gamma_\parallel=T_1^{-1}$ where $T_1=240\times10^{-6}$ s [15,17]. The dynamical behavior predicted by this equation can be explored analytically for small pump modulations. For large pump modulations numerical methods must be used to explore its dependence on frequency and depth of modulation. It is found that the intensities of the two oppositely directed modes may exhibit antiphase periodic, quasiperiodic, and synchronized or unsynchronized chaotic intensity oscillations [14].

For the experiments reported here the drive current of the pump laser was adjusted to 1.5 times the threshold value (pump ratio $r=1.5$). To modulate the gain of the laser a small square-wave component was added to the drive current of the pump laser. The dynamical behavior of the ring laser was explored by varying the frequency ν_m and depth h_m of modulation. For each frequency of modulation, the depth of modulation was varied in the range $[0, r_0=1.5]$. Mode intensities coming out of the laser were monitored by two photodetectors, whose outputs after amplification were recorded by a digital storage oscilloscope for further analyses. The results presented are typical of above-threshold operation of the laser.

Without pump modulation, the mode intensities show antiphase (π out of phase) sinusoidal oscillations. A plot of I_1 vs I_2 produces a straight line $I_1+I_2=$const. Power spectra for both mode intensities show a sharp peak at frequency $b/2\pi$. This allowed us to extract the backscattering coefficient b. Antiphase sinusoidal intensity oscillations are characteristic of single-mode operation of the ring laser and were used as a check for its single-mode operation. All data for a fixed modulation frequency were collected in one session to minimize the variation of backscattering coefficient and cavity decay rate, which were found to vary with the alignment of optical elements inside the cavity and environmental factors such as dust and humidity.

Figure 2 shows experimentally recorded mode intensities $I_1(t)$ and $I_2(t)$ and intensity power spectrum $S(\nu)$ for modulation frequency $\nu_m=2$ kHz and a small depth of modulation $h_m=0.064$. To facilitate comparison between measured and

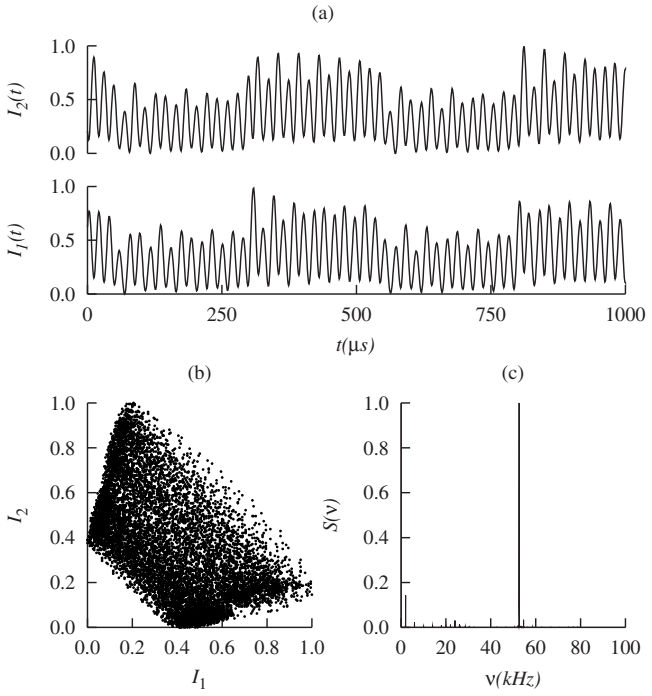

FIG. 2. Experimentally recorded signals for $\nu_m=2$ kHz, $h_m=0.064$, $r_0=1.5$, $b=50$ kHz, and $\delta=2.54\%$: (a) Mode intensities $I_1(t)$ and $I_2(t)$, (b) I_1 vs I_2 plot, and (c) mode intensity power spectrum $S(\nu)$.

theoretically simulated wave forms, intensity wave forms are scaled to have unit maximum intensity and power spectra are normalized to have the highest peak of unit strength. For these parameters, the system exhibits antiphase intensity oscillations but their amplitude is modulated. The power spectrum shows dominant frequencies around $\nu=2$, 24, and 52 kHz. The highest peak corresponds to antiphase intensity oscillations at $b/2\pi$. The effect of small depth of gain modulation $h_m \ll r_0$ is to modulate the amplitude of intensity oscillations at frequency ν_m. This leads to the peak at 2 kHz. Other small peaks at the sum and difference of $b/2\pi$ and ν can also be seen. The third peak at 24 kHz corresponds to the relaxation oscillation frequency for unidirectional operation [18]

$$\nu_r \simeq \frac{1}{2\pi}\sqrt{(r_0-1)\gamma_\parallel\kappa} \tag{6}$$

where r_0 is the average pump parameter and $\gamma_\parallel$ is the population decay rate. The cavity field decay rate $\kappa=c\delta/nL$, where δ is the loss per round trip, L is the cavity perimeter, c is the speed of light, and n is the refractive index. Taking the peak at $\nu=24$ kHz to be the relaxation oscillation frequency ν_r, we can extract the value of δ from

$$\delta = \frac{4\pi^2 nL\nu_r^2}{(r_0-1)\gamma_\parallel c}. \tag{7}$$

Substituting $n=1$, $L=69.6$ cm, $r_0=1.5$, $\gamma_\parallel=4.167$ kHz (for Nd:YAG medium), and $\nu_r=24$ kHz we get $\delta=2.54\%$. This allows us to extract the second parameter $\kappa=\delta c/nL$ needed

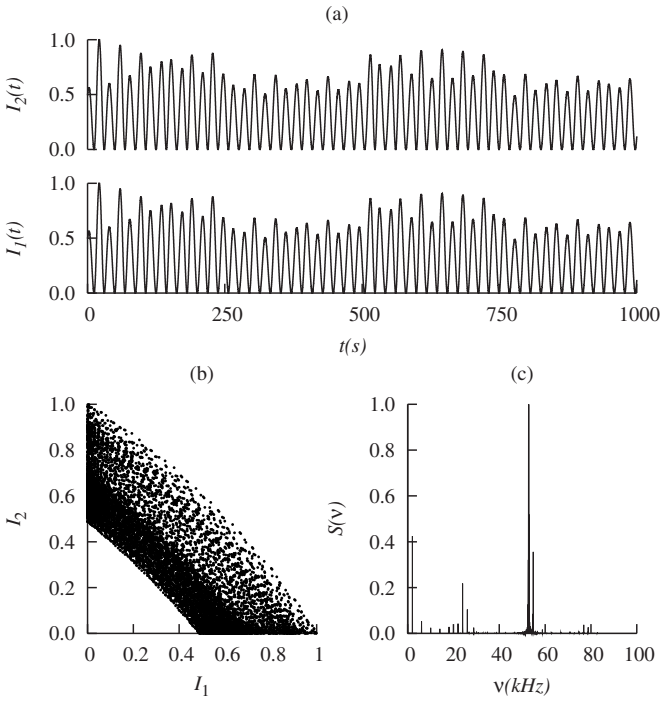

FIG. 3. Theoretically simulated signals for parameters of Fig. 2: (a) Mode intensities $I_1(t)$ and $I_2(t)$, (b) I_1 vs I_2 plot, and (c) mode intensity power spectrum $S(\nu)$.

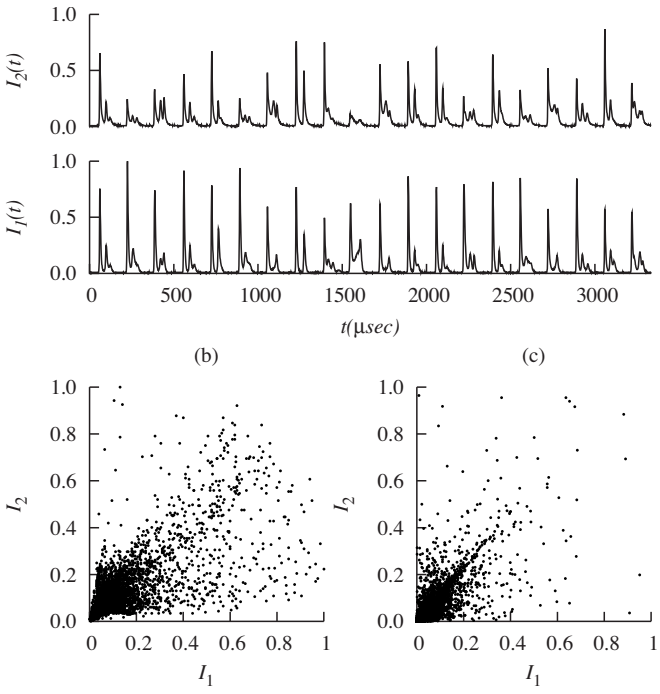

FIG. 4. Experimentally recorded unsynchronized chaotic signals for ν_m=6 kHz and h_m=0.428: (a) Mode intensities I_1 and I_2 and (b) I_1 vs I_2 plot. (c) shows theoretically simulated I_1 vs I_2 plot.

for comparing experimental results with the theoretical predictions.

For bidirectional (single mode in each direction) operation another characteristic frequency associated with relaxation oscillations (in addition to ν_R) appears. This additional frequency is given by $\nu_a=\nu_r/\sqrt{2}$ [19]. The identification of ν_r=24 kHz as the relaxation oscillation frequency is supported by the occurrence of spectral components at ν_r and $\nu_a=\sqrt{2}\nu_r$ together in the power spectra. Indeed in all spectra with low modulation depths, two frequencies close to 24 and 17 kHz ($17\approx 24/\sqrt{2}$) were observed together.

The results of theoretical simulation based on Eqs. (1)–(4) for the parameters of Fig. 2 are shown in Fig. 3 and agree well with experimentally measured quantities. Without gain modulation, I_1 vs I_2 plots of experimentally recorded intensity wave forms, lead to all representative points lying along the line I_1+I_2=const, as expected for antiphase intensity oscillations. In the presence of gain modulation, the amplitude of intensity oscillations is modulated, leading to representative points falling in a band around I_1+I_2=const as seen in Figs. 1 and 2. With increasing depth of modulation, the band in Fig. 2 expands to fill the region near the origin. Intensity modulation becomes increasingly anharmonic as its amplitude increases until at a critical depth of gain nodulation a sudden transition to unsynchronized chaotic oscillations occurs.

The transition to chaos results in dramatic changes in the power spectrum. It is accompanied by the disappearance of the spectral component $b/2\pi$ from the power spectrum, which remains a prominent feature of intensity power spectrum throughout the quasiperiodic regime. In the unsynchronized chaotic regime the intensity wave forms produce I_1 vs I_2 plots with system representative points scattered over a large area (Fig. 4) without any discernible pattern. A regular pattern can, however, emerge for certain parameters although the representative points are still spread out over a significant portion of the I_1-I_2 plane.

It is also possible to operate the laser in the regime where mode intensity wave forms are expected to be chaotic but synchronized to one another [20,21]. Figures 5(a)–5(c) shows experimentally recorded intensity wave forms in this regime corresponding to parameters ν_m=6 kHz, h_m=1.413. For comparison, Fig. 5(c) shows the theoretically expected I_1 vs I_2 plot for these parameters. The representative points corresponding to recorded intensity wave forms crowd around the straight line $I_1=I_2$ in Fig. 5(b). This indicates that, although the wave-form synchronization is lost periodically, the signals do not drift far from synchronization. We attribute the departures from strict synchronization to spontaneous emission and pump noise, which are not included in the theoretical model.

It is difficult to reproduce experimentally measured system trajectories theoretically for chaotic systems because of their sensitive dependence on initial conditions. For this reason we have chosen the maximum Lyapunov exponent for a quantitative comparison between theory and experiment. The maximum Lyapunov exponent is the fastest rate of exponential divergence (or convergence) of nearby system trajectories. It is a global property of the system trajectories rather than finite portions of them. To compute λ_m we need the system trajectory in its full phase space. Experimentally, however, we measure only two dynamic variables (mode intensities). To reconstruct the system trajectory in full phase-space from the measured intensity wave forms, we use a

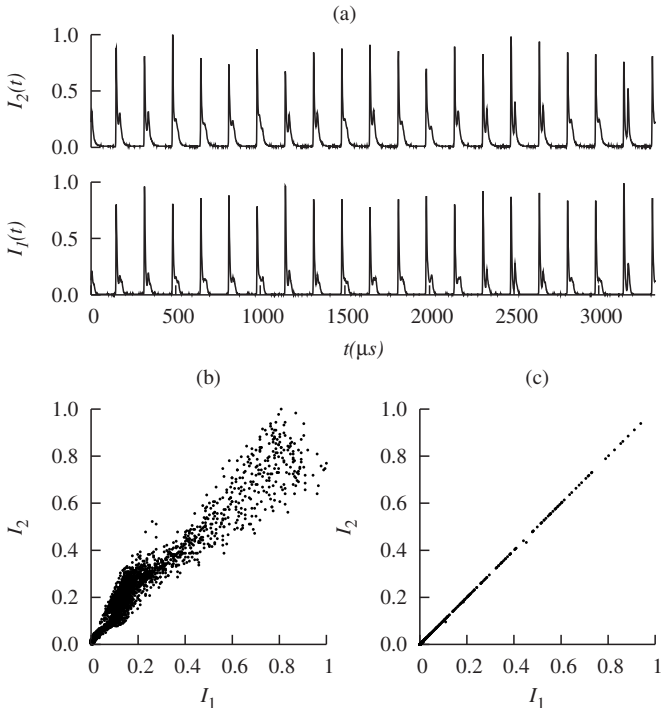

FIG. 5. Experimentally measured intensity wave forms in synchronized chaotic regime for ν_m=6 kHz and h_m=1.413: (a) Mode intensities I_1 and I_2 and (b) experimentally recorded I_1 vs I_2 plot. (c) shows theoretically simulated I_1 vs I_2 plot.

procedure developed by Wolf *et al.*[22]. From the reconstructed phase space we estimate λ_m. Both the experimentally measured and theoretically calculated intensity time series were treated using this procedure. It is important to emphasize that only two parameters κ and b are needed as input to the theoretical model to simulate the experimental results. These parameters were estimated from two characteristic frequencies of the system, viz., the frequency of relaxation oscillations and the frequency of sinusoidal antiphase intensity oscillations. The maximum Lyapunov exponent estimated by using this procedure for ν_m=2 kHz and h_m in the range [0, 1.5] is shown in Fig. 6.

The solid line connecting the experimental points and the dashed line connecting the theoretical points are drawn as guides to the eye. There is reasonable agreement between the values of λ_m calculated from the experimental and theoretical signals. In particular, the peak near h_m=0.39 is well reproduced. This behavior of λ_m could not have been inferred from either the power spectrum or intensity time series.

The system of two strongly coupled laser modes discussed here supports only anticorrelated single-mode operation when population dynamics are slave to the field dynamics [23]. With increased phase space due to population dynamics, the system can accommodate much richer dynamical behavior including synchronized and unsynchronized chaotic intensity oscillations. The synchronization of chaos and quasiperiodic behavior observed here arise naturally by an organization of the internal system dynamics.

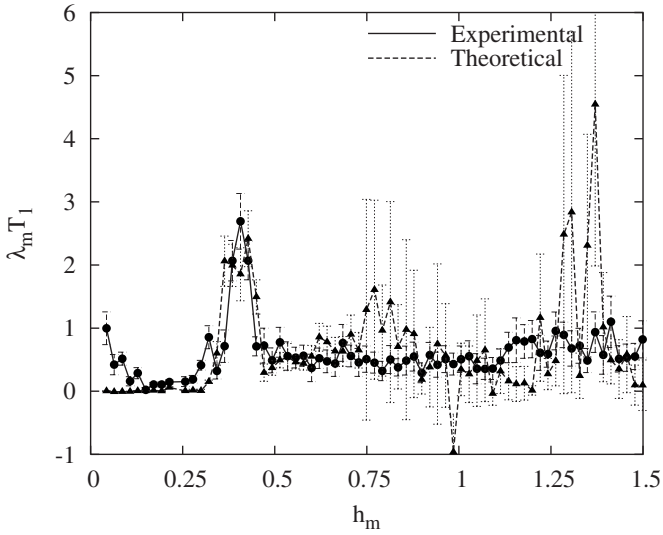

FIG. 6. Maximum Lyapunov exponent as a function of modulation depth calculated from the experimental (circles) and theoretical (triangles) time series for ν_m=2 kHz.

The spectrum of dynamical behavior that a single-mode bidirectional ring laser is capable of exhibiting is extremely rich [24,25]. For example, with the inclusion of polarization dynamics (in addition to cavity and population dynamics) the phase space extends beyond that encountered in class-*B* lasers, leading to the observation of the period-doubling route to chaos, chaotic mode alteration, and antiphase dynamics [26,27].

There is growing interest in extending the concept of synchronization, which originally referred to periodic oscillations, to irregular chaotic oscillations. The general framework for describing and understanding synchronization in the context of chaotic systems is an evolving field of research. The experimental system described here, together with the theoretical model to simulate its rich dynamical behavior, offers exciting opportunities for exploring various concepts in chaos synchronization, including the effects of noise on loss synchronization and perhaps even ways of overcoming the effects of noise in loss of synchronization.

One of us (F.R.) would like to thank E. G. Lariontsev for many helpful exchanges on the work reported here.

[1] Robert C. Hilborn, *Chaos and Nonlinear Dynamics: An Introduction for Scientists and Engineers* (Oxford University Press, New York, 1994); A. A. Tsonis, *Chaos: From Theory to Applications* (Plenum Press, New York, 1992).

[2] E. Ott, C. Grebogi, and J. A. Yorke, Phys. Rev. Lett. **64**, 1196 (1990).

[3] K. Pyragas, Phys. Lett. A **170**, 421 (1992).

[4] G. W. Wei, M. Zhan, and C.-H Lai, Phys. Rev. Lett. **89**,

284103 (2002).
[5] L. M. Pecora and T. L. Carroll, Phys. Rev. Lett. **80**, 2109 (1998).
[6] T. Shinbrot, C. Grebogi, E. Ott, and J. A. Yorke, Nature (London) **363**, 411 (1993); R. Roy, T. W. Murphy, T. D. Maier, Z. Gills, and E. R. Hunt, Phys. Rev. Lett. **68**, 1259 (1992); J. N. Blakely, L. Illing, and D. J. Gauthier, *ibid.* **92**, 193901 (2004).
[7] W. L. Ditto, S. N. Rauseo, and M. L. Spano, Phys. Rev. Lett. **65**, 3211 (1990).
[8] A. Pikovsky, M. Rosenblum, and J. Kurths, *Synchronization* (Cambridge University Press, Cambridge, U. K., 2003); Steven Strogatz, *Sync: The Emerging Science of Spontaneous Order* (Hyperion, New York, 2003).
[9] S. Boccaletti, J. Kurths, G. Osipov, D. L. Valladares, and C. Zhou, Phys. Rep. **366**, 1 (2002).
[10] N. F. Rulkov, Chaos **6**, 262 (1996).
[11] G. D. VanWiggeren and R. Roy, Science **279**, 1197 (1998).
[12] V. Petrov, V. Gaspar, J. Masere, and K. Showalter, Nature (London) **361**, 240 (1993).
[13] G. M. Hall and D. J. Gauthier, Phys. Rev. Lett. **88**, 198102 (2002); A. Garfinkel, M. L. Spano, W. L. Ditto, and J. N. Weiss, Science **257**, 1230 (1992).
[14] F. Rawwagah and Surendra Singh, J. Opt. Soc. Am. B **23**, 1785 (2006).
[15] D. N. Klimenko, N. V. Kravtsov, E. G. Lariontsev, and V. V. Firsov, Quantum Electron. **27**, 631 (1997).
[16] E. G. Lariontsev, Opt. Express **2**, 198 (1998).
[17] W. Koechner, *Solid-State Laser Engineering* (Springer-Verlag, New York, 1988), pp. 48–55.
[18] A. Siegman, *Lasers* (University Science Books, Mill Valley, CA, 1986), Chap. 25.
[19] I. I. Zolotoverkh, N. V. Kravtsov, N. N. Kravtsov, E. G. Lariontsev, and A. A. Makarov, Quantum Electron. **27**, 621 (1997).
[20] L. A. Kotomtseva, E. G. Lariontsev, and S. N. Chekina, Chaos **13**, 279 (2003).
[21] E. G. Lariontsev, Quantum Electron. **28**, 392 (1998).
[22] A. Wolf, J. B. Swift, H. L. Swinney, and J. A. Vastano, Physica D **16**, 285 (1985); A. Wolf, Computer codes FET and BASGEN (Department of Physics, The Cooper Union, 2007), http://www.cooper.edu/~wolf/chaos/chaos.htm
[23] P. Lett, W. Christian, S. Singh, and L. Mandel, Phys. Rev. Lett. **47**, 1892 (1981); S. Singh and L. Mandel, Phys. Rev. A **20**, 2459 (1979).
[24] H. Zeghlache, P. Mandel, N. B. Abraham, L. M. Hoffer, G. L. Lippi, and T. Mello, Phys. Rev. A **37**, 470 (1988).
[25] L. M. Hoffer and N. B. Abraham, Opt. Commun. **74**, 261 (1989); M. Clerc and P. Coullet, Phys. Rev. E **60**, 6589 (1999).
[26] G. Lippi, J. Tredicce, N. Abraham, and F. Arecchi, Opt. Commun. **53**, 129 (1985).
[27] D. Y. Tang, R. Dykstra, and N. R. Heckenberg, Opt. Commun. **126**, 318 (1996); Phys. Rev. A **54**, 5317 (1996).